Fringe modulation skewing effect in white-light vertical scanning interferometry

Akiko Harasaki and James C. Wyant

An interference fringe modulation skewing effect in white-light vertical scanning interferometry that can produce a batwings artifact in a step height measurement is described. The skewing occurs at a position on or close to the edge of a step in the sample under measurement when the step height is less than the coherence length of the light source used. A diffraction model is used to explain the effect. © 2000 Optical Society of America

OCIS codes: 120.6650, 120.6660, 180.3170.

1. Introduction

One method of determining surface height involves the use of a broad-spectral-width light source in an interferometer and measurement of the degree of modulation contrast as a function of path difference.[1–15] Because of the large spectral bandwidth of the source, the coherence length of the source is short, so good contrast fringes will be obtained only when the two paths of the interferometer are closely matched in length. By looking at the sample position for which the fringe contrast is a maximum while the optical path difference is varied, one can determine the height variations across the sample. In this measurement there are no height ambiguities or focus errors because the interferometer is adjusted such that the sample is in focus when the optical path difference is zero. Many excellent features of white-light vertical scanning interferometry were published previously.[1–15]

Although this is a good technique for measuring many surfaces, it does not work especially well with step heights[16] that are less than the coherence length of the light source in use. The problem has been known as batwings because of the shape of the false information. To our best knowledge, the batwings show up for every well-established white-light vertical scanning technique. In Section 2 we explain the exact nature of batwings in the and discuss the skewing of coherence envelopes in correlograms, which are the interference intensity distribution along the vertical scanning direction. A diffraction model to explain this effect is proposed in Section 3.

2. Batwings

Surface profiles of 80-nm, 460-nm, and 1.7-μm step height-standards (VLSI Standards, Inc.) measured with the white-light vertical scanning technique are shown in Fig. 1. The light source used in the measurement has a coherence length of 1.2 μm. Batwings clearly appear in profiles of the 80- and 460-nm step-height standards but not in the 1.7-μm standard, whose step height exceeds the coherence length of the light source. The top portion close to the edge of the step discontinuity, whose height is less than the coherence length, always appears higher and the bottom portion appears lower than it actually is. From Fig. 1 it is clear that the reason that the false information is named batwings is its appearance. The 80-nm height standard can also be measured with phase-shifting interferometry; in that case the false information does not appear. Phase-shifting interferometric measurement of the 80-nm height standard is shown in Fig. 2. The result suggests that the false information has more effect on intensity than on phase, and this may give us a hint of a way to solve the problem.[17] Table 1 summarizes the results obtained from careful measurements of gratings with several periods and depths. The first two rows in the table tell us that the batwings appear only when the coherence length of the light source is larger than the step discontinuity. The third and fourth parameters are essentially the same, because the higher-magnification interference-microscope ob-

The authors are with the Optical Sciences Center, University of Arizona, Tucson, Arizona 85721. A. Harasaki's e-mail address is (harasaki@u.arizona.edu).

Received 7 September 1999; revised manuscript received 13 January 2000.

0003-6935/00/132101-06$15.00/0

© 2000 Optical Society of America

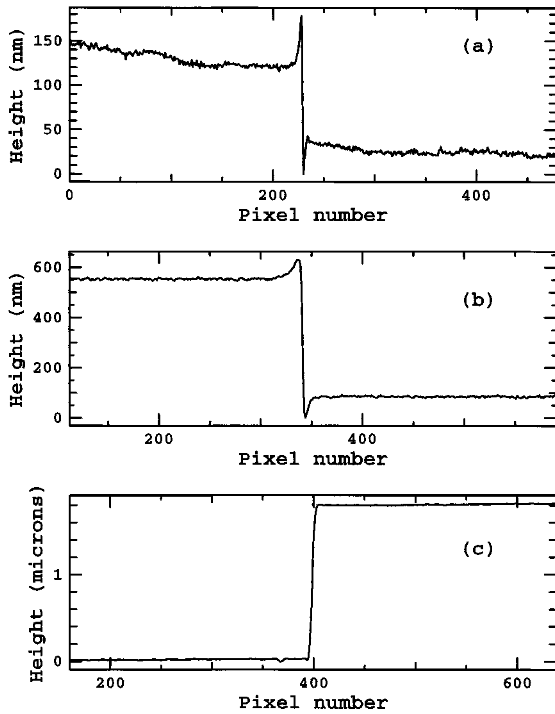

Fig. 1. Profiles of (a) the 80-nm step-height standard, (b) the 460-nm step-height standard, (c) the 1.7 μm step-height standard measured with a Mirau interference microscope.

jective has a larger numerical aperture (N.A.). The N.A. of the objective determines the cutoff spatial frequency of the system. As shown in Fig. 1, the batwings contain high spatial components, so high N.A. permits large batwings. That the number of data points along the vertical scanning direction changes the batwings effect strongly suggests that we investigate the correlogram, which might be deformed at the positions that have batwings. The result that a short grating period increases the height of batwings can be explained by the signal-to-noise ratio. It is expected that more light will be trapped in the grating wells when the period gets small with the same depth. Anything happening on or near the step edges that provides false information enhances

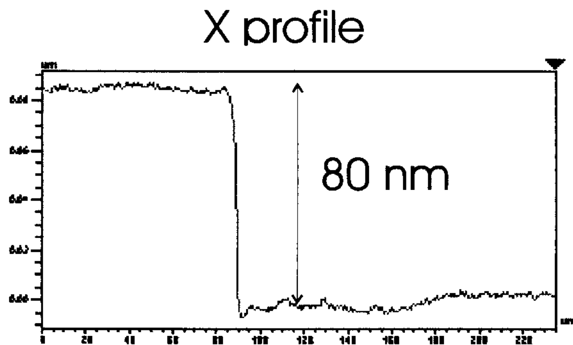

Fig. 2. Profile of the 80-nm step-height standard measured by the phase-shifting technique.

Table 1. Influences of Measurement Parameters on Batwings[a]

Parameter	Description
Wavelength	Shorter → narrow the width of the batwings.
Grating depth	Very strong up to several hundred nanometers; not much when larger than 1 μm.
Objective magnification	Higher magnification → more batwings.
N.A.	Larger N.A. → more batwings.
Data points	Containing many defocus frames → the height of the batwings increases.
Grating period	Short period → the height of the batwings increases.

[a]One calculates the profile by locating the centroid of correlogram.[17]

the effects when the signal light carrying the information decreases.

The surface-height information is retrieved from the modulation contrast of the correlograms. The correlograms at the positions of the batwings would give us good insight into the phenomenon. Figures 3–5 show the correlograms for the 80-nm, 460-nm, and 1.7-μm step-height standards along a line across the step discontinuity. First we notice the fringe contrast reduction at positions on or close to the step

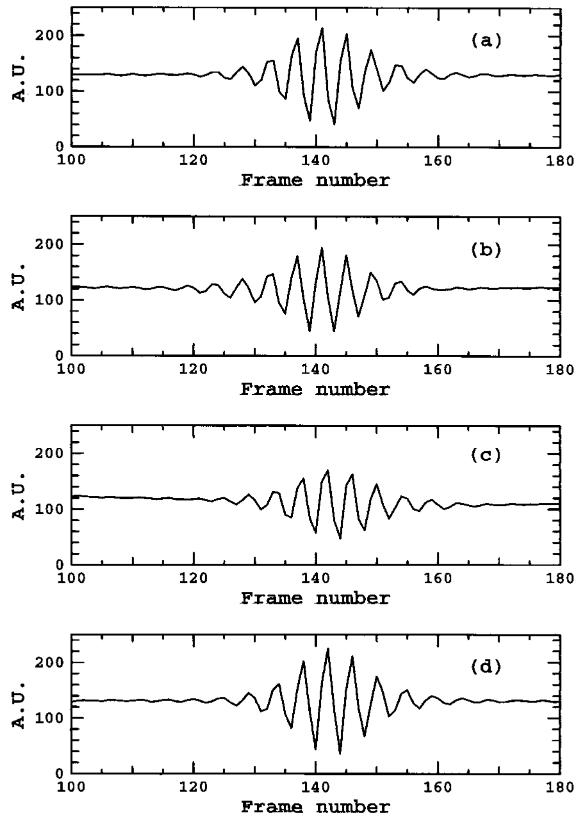

Fig. 3. Correlograms of the 80-nm height standard across the step discontinuity (a) far from the edge on the top side, (b) close to the edge on the top side, (c) close to the edge on the bottom side, (d) far from the edge on the bottom side.

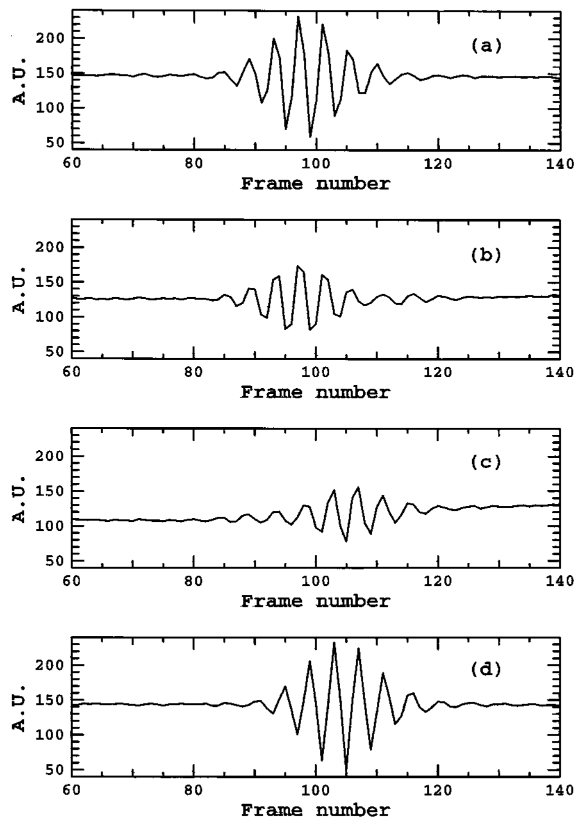

Fig. 4. Correlograms of the 460-nm height standard across the step discontinuity (a) far from the edge on the top side, (b) close to the edge on the top side, (c) close to the edge on the bottom side, (d) far from the edge on the bottom side.

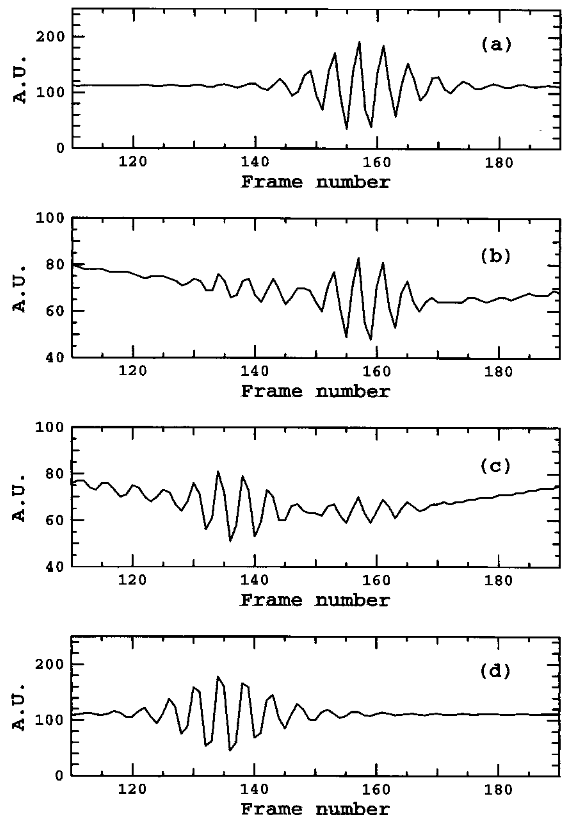

Fig. 5. Correlograms of the 1.7-μm height standard across the step discontinuity (a) far from the edge on the top side, (b) close to the edge on the top side, (c) close to the edge on the bottom side, (d) far from the edge on the bottom side.

edge owing to the decrease of light reflected back to the system from the sample surface. The integrating energy distributions across the step standards are shown in Fig. 6 to illustrate the effect. The light that comes back to the system decreases as the step height increases. The contrast reduction from the decrease of test beam intensity results in a poor signal-to-noise ratio, but it does not directly cause the batwings because batwings do not appear in the measured surface profile of the 1.7-μm step-height standard, which suffers the greatest energy reduction.

We determine the surface heights either by locating the modulation-contrast peak position by using the least-squares fitting method[10] to the discrete data points or by calculating the centroid[4,6,17] of the contrast. Usually the latter procedure takes less time[17]; therefore it saves computing power. From Figs. 3 and 4 we can clearly see that the peak and the centroid are not necessarily coincident if there is noise in the correlogram. Also, at positions close to the edge on the top (bottom) side the peak and the centroid are moving toward larger (smaller) frame positions than where they should be. In addition, the position of the centroid shifts more than the position of the modulation peak does. This explains why including more defocus data points could increase the height of batwings.[10,16] For simple white-light two-beam interference, the fringe modulation contrast is Gaussian when the light source has a Gaussian distribution, as in this case, but it somehow skews at positions close to the edges. We can imagine that the diffraction effect from the edge changes the effective reflectivity from the sample and deforms the modulation contrast when the step height is smaller than the coherence length of the light source. In Section 3 we show that diffraction by two shifted apertures can cause batwings.

3. Diffraction Model

We model the step edge as two shifted apertures, as illustrated in Fig. 7, assuming a plane wave normally incident upon the step edge and reflecting back to the system after it is diffracted by the edge. When the step height is less than the coherence length of the illumination light source, the diffracted and reflected beams from the top and the bottom sides of the step edge interfere with each other and travel back to the system. The Mirau objective collects the light amplitude at the focal plane that interferes with the reference beam. The objective transmits only the amplitude distribution of the spatial frequencies that is lower than $\lambda/\mathrm{N.A.}$; λ is the wavelength. When one is using a white-light source, the intensity collected by the CCD array is the sum of the intensities of all the wavelengths contained in the white-light source.

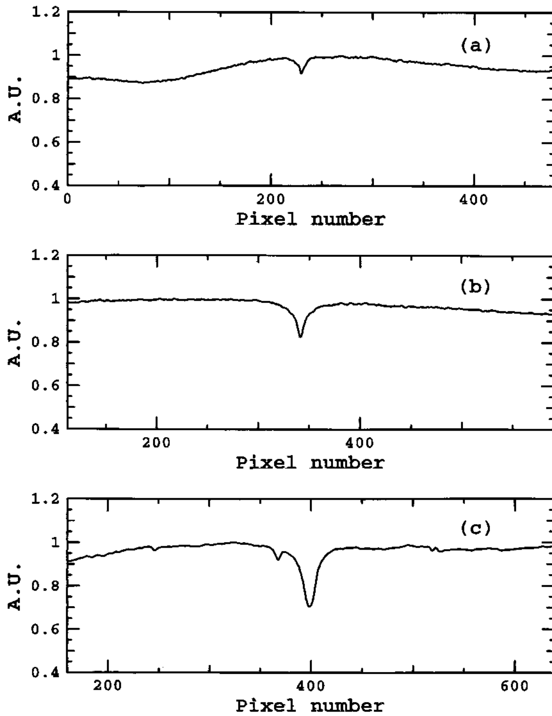

Fig. 6. Integrating energy of (a) the 80-nm step-height standard, (b) the 460-nm step-height standard, (c) the 1.7-μm step-height standard across the step discontinuity.

We are trying to calculate the diffraction light amplitude at a distance that is much less than one wavelength, so the Fresnel approximation is not valid. If we limit ourselves to propagation between parallel planes, the rigorous diffraction equation can be expressed as[18]

$$u(x, y, z) = \int_{-\infty}^{\infty}\int_{-\infty}^{\infty} u(x_0, y_0, z = 0) \times u_{ph}(x - x_0, y - y_0, z)\mathrm{d}x_0\mathrm{d}y_0, \quad (1)$$

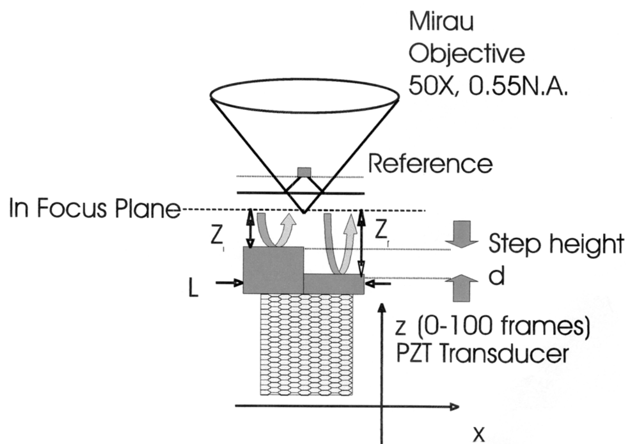

Fig. 7. Schematic configuration of a Mirau interference microscope and a step-edge sample: PZT, piezoelectric.

where u_{ph} is the pinhole wave:

$$u_{ph}(x, y, z) = -\frac{1}{2\pi}\frac{\partial}{\partial z}\left[\frac{\exp(ikr)}{r}\right], \quad (2)$$

k is the wave number, and $r = (x^2 + y^2 + z^2)^{1/2}$. $u(x, y, z)$ is the complex amplitude of the diffracted light at a distance z from the aperture plane; $u(x_0, y_0, z = 0)$ is the complex amplitude at the aperture plane. Because Eq. (1) is in the form of a convolution, Fourier transforming the equation leads to a simplification of the two-dimensional convolution to a product:

$$U(\xi, \zeta, z) = U(\xi, \zeta, z = 0) \times U_{ph}(\xi, \zeta, z), \quad (3)$$

where $U(\xi, \zeta, z)$, $U(\xi, \zeta, z = 0)$, and $U_{ph}(\xi, \zeta, z)$ are the two-dimensional Fourier transforms of $u(x, y, z)$, $u(x, y, z = 0)$, and $u_{ph}(x, y, z)$, respectively. The Fourier-transformed pinhole wave has a simple form:

$$U_{ph}(\xi, \zeta, z) = \exp\left\{-2\pi i z\left[\frac{1}{\lambda^2} - (\xi^2 + \zeta^2)\right]^{1/2}\right\}, \quad (4)$$

with $z > 0$. By inverse Fourier transforming Eq. (3) we can calculate the diffraction pattern at any plane close to the diffraction aperture. The light is collected by a lens, so in our case there are no evanescent components and the Fourier spectrum needs to be integrated only from $-1/\lambda$ to $1/\lambda$:

$$u(x, y, z) = \int_{-1/\lambda}^{1/\lambda}\int_{-1/\lambda}^{1/\lambda} U(\xi, \zeta, z)\exp[i2\pi(\xi x + \zeta y)]\mathrm{d}\xi\mathrm{d}\zeta. \quad (5)$$

This procedure can easily be done with the help of a fast-Fourier-transform algorithm and a fast computer.

Let us go back to the Mirau interference microscope shown in Fig. 7. The system is essentially one dimensional, or there is no dependence on y direction, so the integral in Eq. (5) can be carried out and

$$u(x, z) = \int_{-1/\lambda}^{1/\lambda} U(\xi, z)\exp(i2\pi\xi x)\mathrm{d}\xi, \quad (6)$$

$$U(\xi, z) = U(\xi, z = 0)\exp\left(-2\pi i z\sqrt{\frac{1}{\lambda^2} - \xi^2}\right). \quad (7)$$

For wavelength λ the Fourier spectrum of the test arm's beam amplitude at the focal plane of the objective is

$$U(\xi, z, \lambda) = [U_l(\xi, z = 0, \lambda)U_{ph}(\xi, z_l, \lambda) + U_r(\xi, z = 0, \lambda)U_{ph}(\xi, z_r, \lambda)] \times \mathrm{rect}\left(\frac{\xi}{\mathrm{N.A.}/\lambda}\right). \quad (8)$$

U_l and U_r are the Fourier transforms of amplitudes u_l and u_r from the left and right sides, respectively, of the step in Fig. 7:

$$u_l(x, z_l, \lambda) = a_l \exp\left(-i \frac{2\pi}{\lambda} z_l\right) \mathrm{rect}\left(\frac{x - L/4}{L/2}\right), \quad (9)$$

$$u_r(x, z_r, \lambda) = a_r \exp\left(-i \frac{2\pi}{\lambda} z_r\right) \mathrm{rect}\left(\frac{x - 3L/4}{L/2}\right); \quad (10)$$

L is the lateral extension of the step sample. Figure 7 shows $z_l = z$ and $z_r = z + d$. a_l and a_r are the relative amounts of light that the objective collects from the left and right sides, respectively, of the step. For the positions close to the edge on left side, $a_l > a_r$, and vice versa. The rectangular function represents the coherent optical transfer function of the objective. The test arm beam interferes with the reference beam, and the detector sees the intensity

$$I(x, z) = \int_{\lambda_1}^{\lambda_2} \left| u(x, z, \lambda) + \mathrm{rect}\left(\frac{x - L/2}{L}\right) \right|^2 \mathrm{d}\lambda. \quad (11)$$

We carried out Eq. (11) numerically. The number of sampling points in the lateral direction is $N = 1024$, and the sampling distance is $\Delta x = 1.2$ μm, so the total lateral extension is $L = 1.2276$ mm in our simulation. The largest spatial frequency here is $\xi_{\max} = 1/\Delta x = 834$ lines/mm, so up to a wavelength of 660 nm all frequencies go through the bandpass filter set by the objective. The Mirau interference microscope that we used to collect data for Figs. 1–5 operates at a center wavelength of 600 nm when an unfiltered tungsten light bulb is used as a white-light source. To meet this condition we chose a flat wavelength distribution from $\lambda_1 = 540$ nm to $\lambda_2 = 660$ nm in our simulation, and we can eliminate the rect function from Eq. (8), which will make the calculation much simpler. The interference microscope moves the objective or the sample stage in 80-nm steps and sends CCD images to the computer through the entire vertical scanning range. We set the sampling distance in the axial direction to be $\Delta z = 80$ nm as in the real case. Figures 8(a) and 8(b) show simulated correlograms of the top portion of the 460-nm height standard with the step height set at $d = 460$ nm and the relative light ratio from the left side (top, [0, 510]), $a_l = 2$ and the right side (bottom, [514, 1023]), $a_r = 1$. $a_l = 1.5$ and $a_r = 0.5$ are used for the boundary positions $x = [511, 513]$ such that the objective collects light from both sides. By setting $a_l = 1$ for the positions $x = [0, 510]$, $a_r = 2$ for positions $x = [514, 1023]$ and $a_l = 0.5$, $a_r = 1.5$ for boundary positions $x = [511, 513]$, we can calculate the bottom side correlograms as well [Figs. 8(c) and 8(d)]. The best focus frame calculated from the correlograms by the centroid approach[17] is shown in Fig. 9. The simulated correlograms clearly possess the properties of the measured correlograms: the energy and modulation contrast decrease and the modulation contrast envelope skews at positions close to the step edge. Consequently the profile calculated with the same

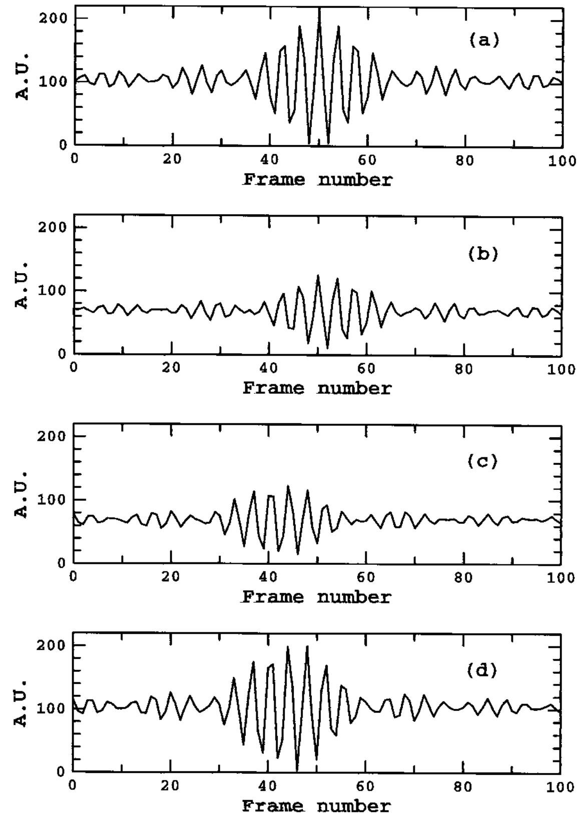

Fig. 8. Simulated correlograms of the 460-nm height standard (a) far from the step edge on the top side, (b) close to the step edge on the top side, (c) close to the step edge on the bottom side, (d) far from the step edge on the top side.

algorithm shows significant bat wings. The simulation results can be explained as follows:

(1) The objective collects light from an area that has an Airy-disk diameter (1.22 λ/N.A.) extension. At positions close to the step edge, part of the light comes from the top portion of the step edge and the other part comes from the bottom portion of the edge. If the CCD array pixel sees the top (bottom) part close to the edge, there is relatively more light reflected and diffracted back to the system from the top (bottom) part.

(2) When the step height is less than the coherence length of the white-light source, the light from the top

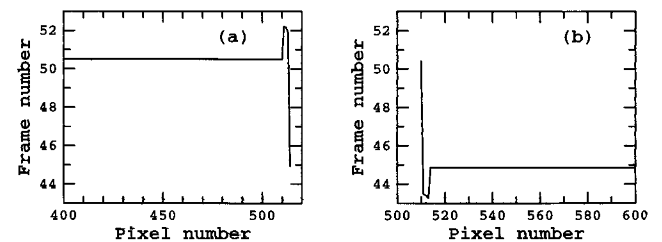

Fig. 9. Calculated best focus frame of the 460-nm height standard: (a) the top portion close to the step edge and (b) the bottom portion close to the step edge.

portion and that from bottom portion interfere with each other. As a result, the fringe modulation envelope skews so both the peak position and the centroid shift away.

(3) Constructing the surface profile by locating the peak position or the centroid of the modulation contrast produces batwings.

We have to mention a few things about the measurement results of the 1.7-μm height standard. The correlograms of the positions close to the step edge in Fig. 5 clearly show two coherence envelopes shifted off approximately the distance of the step height. The two envelopes can be explained as being two independent interference phenomena, i.e., interference of the test beam from the top portion and the reference beam and interference of the test beam from the bottom portion and the reference beam. The contrasts of the two interference patterns give us the intensity ratio of the light from the top and the bottom of the step edge. Because the step height exceeds the coherence length of the white-light source, the reflected and diffracted light from the top of the step edge and that from the bottom of the step edge do not interfere with each other. We point out that in this case the profile [Fig. 1(c)] from the correlogram's centroid does not show batwings, but it does not give the correct surface height at the positions close to the step edge either. The centroid is located at the frame position between the two coherence envelopes; it is not the actual height position. Locating the larger peak from the two envelopes gives a better estimation of the surface height because it is the surface height where the objective collects more light. A detailed discussion of location of the coherence envelope peak and centroid is given in Ref. 10.

4. Conclusions

The batwing effect that affects all white-light vertical scanning techniques in interference microscopes and the fringe contrast envelope skewing effect have been discussed. A diffraction model was given to explain envelope skewing close to the step discontinuity when the step height is less than the coherence length of the source. The model has successfully simulated envelope skewing and batwings.

The authors thank Erik Novak and Joanna Schmit of Veeco Corporation for valuable and interesting suggestions and discussions.

References and Notes

1. N. Balsubramanian, "Optical system for surface topography measurement," U.S. patent 4,340,306 (20 July 1982).
2. M. Davidson, K. Kaufman, I. Mazor, and F. Cohen, "An application of interference microscope to integrated circuit inspection and metrology," in *Integrated Circuit Microscopy: Inspection and Process Control*, K. M. Monahan, ed., Proc. SPIE **775,** 233–247 (1987).
3. B. S. Lee and T. C. Strand, "Profilometry with a coherence scanning microscope," Appl. Opt. **29,** 3784–3788 (1990).
4. G. S. Kino and S. S. C. Chim, "Mirau correlation microscope," Appl. Opt. **32,** 3438–3783 (1990).
5. D. K. Cohen, P. J. Caber, and C. P. Brophy, "Rough surface profiler and method," U.S. patent 5,133,601 (28 July 1992).
6. S. S. C. Chim and G. S. Kino, "Three-dimensional image realization in interference microscopy," Appl. Opt. **31,** 2550–2553 (1992).
7. P. J. Caber, "Interferometric profiler for rough surfaces," Appl. Opt. **32,** 3438–3441 (1993).
8. L. Deck and P. de Groot, "High-speed noncontact profiler based on scanning white-light interferometry," Appl. Opt. **33,** 7334–7338 (1994).
9. P. Hariharan and M. Roy, "White-light phase-stepping interferometry: measurement of the fractional interference order," J. Mod. Opt. **42,** 2357–2360 (1995).
10. K. G. Larkin, "Effective nonlinear algorithm for envelop detection in white light interferometry," J. Opt. Soc. Am. A **13,** 832–843 (1996).
11. J. C. Wyant and J. Schmit, "Computerized interferometric measurement of surface microstructure," in *Optical Inspection and Micromeasurements*, C. Gorecki, ed., Proc. SPIE **2782,** 26–37 (1996).
12. P. Sandoz, "Wavelet transform as a processing tool in white-light interferometry," Opt. Lett. **22,** 1065–1067 (1997).
13. P. Sandoz, R. Devillers, and A. Plata, "Unambiguous profilometry by fringe-order identification in white-light phase-shifting interferometry," J. Mod. Opt. **44,** 519–534 (1997).
14. R. J. Recknagel and G. Notni, "Analysis of white light interferograms using wavelet methods," Opt. Commun. **148,** 122–128 (1998).
15. M. Hart, D. G. Vass, and M. L. Begbie, "Fast surface profiling by spectral analysis of white-light interferograms with Fourier transform spectroscopy," Appl. Opt. **37,** 1764–1769 (1998).
16. A. Harasaki, J. Schmit, and J. C. Wyant, "Improved vertical-scanning interferometry," Appl. Opt. **39,** 2107–2115.
17. Estimating the centroid of function $m(i)[x, y] = \{I(i)[x, y] - I(i-1)[x, y]\}^2$ gives the surface height $h[x, y]$ at lateral position $[x, y]$, where $I(i)[x, y]$ is the intensity of vertical scanning position i in a correlogram for scanning steps of 90° and 270°. It can easily be shown that

$$\bar{z} = \frac{\sum_i im(i)[x, y]}{\sum_i m(i)[x, y]} = h + \frac{\Gamma'(4/\lambda)\cos[2\pi(4/\lambda)h]}{2\pi\{\Gamma(0) + \Gamma(4/\lambda)\sin[2\pi(4/\lambda)h]\}}$$

for the symmetric coherence function, where Γ and Γ' are the Fourier transform of the coherence function and its first derivative, respectively, and $\bar{\lambda}$ is the mean wavelength of the white-light source. From knowledge of the coherence function we know that the second term is very small; thus the centroid of function $m(i)$ is a good estimator of surface height h.
18. A. Jendral and O. Bryngdahl, "Synthetic near-field holograms with localized information," Opt. Lett. **20,** 1204–1206 (1995).